



Discovery of a series of ruthenium(II) derivatives with α -dicarbonylmonoxime as novel inhibitors of cancer cells invasion and metastasis

Yihui He, Huiying Xue, Wendian Zhang, Li Wang, Guangya Xiang, Lei Li^{**}, Xianmei Shang^{*}

Tongji School of Pharmacy, Huazhong University of Science and Technology, 13 Hangkong Road, Wuhan 430030, PR China

ARTICLE INFO

Article history:

Received 25 December 2016

Received in revised form

2 May 2017

Accepted 10 May 2017

Available online 11 May 2017

Keywords:

Ruthenium(II) complexes

Synthesis

Cytotoxicity

Anti-metastasis

ABSTRACT

A series of novel ruthenium(II)-cymene complexes (**1–9**) with substituted α -dicarbonylmonoximes of general formula $[\text{Ru}(\eta^6\text{-cymene})(\text{L})\text{Cl}]$ ($\text{L} = \text{N,O}$ -chelating bidentate α -dicarbonylmonoxime derivatives) have been synthesized and characterized by elemental analysis, IR, ^1H NMR, ^{13}C NMR spectroscopies, and in three cases by single crystal X-ray diffraction analysis. The most effective compound **9** displays remarkable anti-invasion and anti-metastasis properties without apparent cytotoxicity toward three different human cancer cell lines (MCF-7, Hela and HepG2). Further protein level studies suggest that the anti-metastasis activity of the complexes may result from the increasing expression of E-cadherin and reducing expression of Vimentin.

© 2017 Elsevier B.V. All rights reserved.

1. Introduction

The discovery of the anticancer properties of cisplatin in the 1960s was a breakthrough event in metal-based drugs field [1,2]. Since then a tremendous number of novel metal complexes have been synthesized and evaluated to find species with better anticancer properties, lower toxic side effects, and less tumor resistance to cisplatin [3–6]. Of the alternatives to platinum-based anticancer drugs, most progress has been made with agents based on ruthenium that tend to exhibit fewer side effects than platinum-based complexes [7–13], and so far, three ruthenium(III) compounds, NAMI-A [14], KP1019 [15] and KP1339 [16] have already reached phase II clinical trials, by displaying antitumor activity against primary tumors and metastasis, and showing low toxicity and favorable clearance properties [17,18].

In addition to Ru(III) compounds, Ru(II)-arene complexes have been demonstrated great therapeutic potential, although none of these compounds has yet entered clinical trials [11,19]. In our previous studies a series of ruthenium(II)-*p*-cymene complexes containing oxamate ligands coordinated in a bidentate O, O-donors

manner were synthesized and characterized [20], and all complexes exhibited very strong *in vitro* protein tyrosine kinase inhibitory activity with IC_{50} values in the range of 0.02–3.11 μM . Tyrosine kinases are important cellular signaling proteins that have a variety of biological activities including cell proliferation and migration. Inhibition of angiogenic tyrosine kinases has been developed as a systemic treatment strategy for cancer, and three anti-angiogenic tyrosine kinase inhibitors (sunitinib, sorafenib and pazopanib) have been approved for treatment of patients with advanced cancer on account of excellent anti-metastasis effect [21].

The epithelial-mesenchymal transition (EMT) program broadly regulates invasion and metastasis, and E-cadherin (a key cell-to-cell adhesion molecule) and vimentin are important markers of EMT [22], so the anti-metastasis action concerned relevant protein expression level studies. As an extension of our previous research on Ru(II)-*p*-cymene complexes with oximate ligands, with the reports that some oxime organic derivatives have anticarcinogenic activities and the amino-oxime Ru(II) complexes (having bidentate N, N-donors) have shown to modulate both adhesion and migratory capabilities of PC-3 cells [26], we are interested in the properties of the Ru(II)-*p*-cymene complexes with oxime ligands. Because the binding mode of the oxime group depends to a great extent on the presence of a neighboring donor group in the same ligand, and the α -dicarbonylmonoximes have bidentate O, N-donors and constitute very important of chelating agents with

* Corresponding author.

** Corresponding author.

E-mail addresses: leileisure@163.com (L. Li), shangxianmei@hust.edu.cn (X. Shang).

bioactivity [23,24], we are wondering if the ruthenium complexes with this special kind of monoximes show anti-invasion and anti-metastasis activity.

In the current work, we will combine ruthenium-*p*-cymene units with α -dicarbonylmonoxime ligands to generate a series of new organo-ruthenium(II) compounds, and the antitumor activity of ruthenium(II)-cymene-dicarbonylmonoxime complexes will be evaluated. The apoptosis and the cell cycle arrest will be investigated by flow cytometry for the antiproliferative mechanism. Scratch wound healing assay and transwell studies will also be investigated on the migration and invasive of human cancer cells for anti-metastasis effect. Further protein level research will be carried out by western blot analysis for preliminary anti-invasion and anti-metastasis mechanism.

2. Results and discussion

2.1. Synthesis of the $[\text{Ru}(\eta^6\text{-}p\text{-cymene})(\text{L})\text{Cl}]$ complexes

The synthesis of the title compounds (**1–9**) is as outlined in Scheme 1. A series of new ruthenium(II) complexes $[(\eta^6\text{-}p\text{-cymene})\text{Ru}(\text{L})\text{Cl}]$ ($\text{L} = \text{N,O}$ -chelating α -dicarbonylmonoxime derivatives) have been prepared by the reaction of $[\text{RuCl}(\eta^6\text{-}p\text{-cymene})(\mu\text{-Cl})_2]$ with the appropriate α -diketone monoxime in methanol at room temperature. Compounds **1–9** are solids with intense colors, all of which are stable when exposed to moist air. They are freely soluble in DMSO, dichloromethane or chloroform and soluble in alcohols, but insoluble in water.

2.2. Spectral studies

The elemental analysis data of the complexes are in good agreement with the calculated values. In the IR spectra of the ligands, the stretching vibration bands of O–H appear at 3249–3444 cm^{-1} respectively, and these bands disappear in the spectra of **1–9**, showing the deprotonation of –OH groups [25]. In the spectra of complexes **1–9**, the $\nu(\text{C}=\text{O})$ band (at 1609–1639 cm^{-1}) is shifted to lower frequencies by about 24–70 cm^{-1} compared to free ligands (ν_{CO} for substituted α -diketone monoxime are in the 1663–1726 cm^{-1} range), indicating the coordination of oxygen atom of the carbonyl moiety to Ru(II) ion [25–27]. The striking feature common in all the spectra of the complexes are the noticeable shift of $\nu(\text{N}-\text{O})$ and $\nu(\text{C}=\text{N})$ stretching vibrations relative to the free ligands. This suggests the coordination of the oxime group through nitrogen atom in all complexes. These phenomena indicate that the α -diketone monoxime coordinated with central Ru atom in a N,O-chelating mode.

In the ^1H NMR spectra of **1–9**, the expected resonances are observed for the cymene and the substituted α -diketone monoxime. As a result of the coordination of the substituted bidentate chelate mode unit, downfield shifts (0.10–0.20 ppm) of the ligand protons are observed relative to the free α -diketone monoxime. Similar downfield shifts were also detected for the coordinated *p*-cymene in **1–9** as compared to the cymene ligand in $[\text{RuCl}(\eta^6\text{-}p\text{-cymene})(\mu\text{-Cl})_2]$. The spectra of the complexes **1–9** did not show any signal for N–OH, indicating the deprotonation of oxime proton leaving oxygen uncoordinated (crystal structures will be discussed later). The ^{13}C NMR spectra for **1–9** also show the expected resonance signals.

2.3. X-ray diffraction analysis

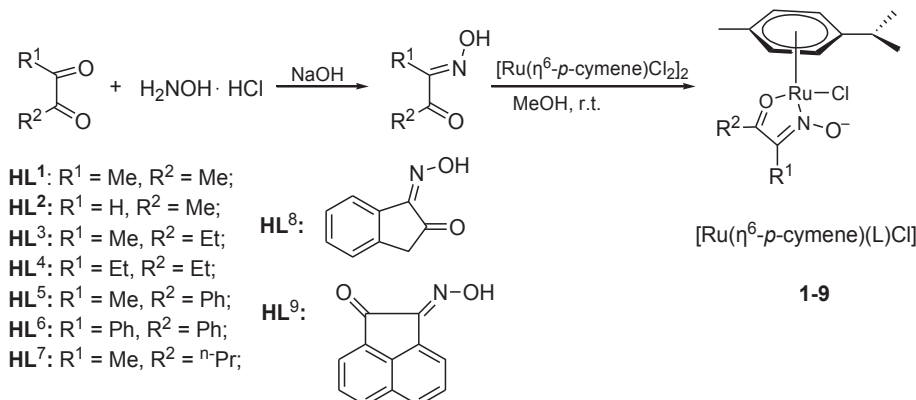
Single crystals were grown from the mixture of dichloromethane– n -hexane by slow evaporation at room temperature or a lower temperature for **1**, **3** and **5**. The crystal structures of **1**, **3** and **5** were determined by X-ray crystallography (see Experimental section for details of the data collections and structure refinements). The molecular structures of **1**, **3** and **5** are illustrated in Figs. 1–3, respectively. The most relevant parameters of bond distances and angles of the complexes are given in the legends of Figs. 1–3.

The X-ray analysis clearly revealed complexes **1**, **3** and **5** adopt the similar three-legged piano-stool coordination geometry around the ruthenium ion. Ru(II) ions are coordinated to carbonyl oxygen and nitrogen of the α -diketone monoxime ligands (HL^1 , HL^3 and HL^5) forming a five-member chelate ring with a mean bite angle of 77° (from $76.87(13)^\circ$ to $77.13(7)^\circ$). The Ru– η^6 -arene centroid distances are 1.680 (**1**), 1.670 (**3**), 1.676 (**5**), suggesting that the ruthenium-cymene interaction is similar for the three ruthenium-cymene complexes with different α -diketone monoxime ligands.

For **1**, **3** and **5**, the Ru–N, Ru–O1, Ru–Cl and Ru–C_{cym} distances are all normal and they are similar to what have been observed in structurally characterized Ru(II) complexes containing these bonds [27–29]. It is important to note that the deprotonation of the oxime ($\text{C}=\text{N}-\text{OH}$) and the coordination of the oxime nitrogen (not oxygen), which results in the shortening of the N–O2 [$1.256(2) \sim 1.282(5) \text{ \AA}$] and C(O1)–C(N) [$1.402(6) \sim 1.411(4) \text{ \AA}$] distances and the lengthening of the C–N distance in the α -ketoxime group. The facts suggest a delocalization of the π electron density on deprotonated side of the α -ketoxime (O1–C–C–N1–O2) moiety.

2.4. Cytotoxicity studies

Eight synthesized ruthenium(II) compounds (**1–5** and **7–9**, **6** not



Scheme 1. Synthesis of the $[\text{Ru}(\eta^6\text{-}p\text{-cymene})(\text{L})\text{Cl}]$ complexes (**1–9**).

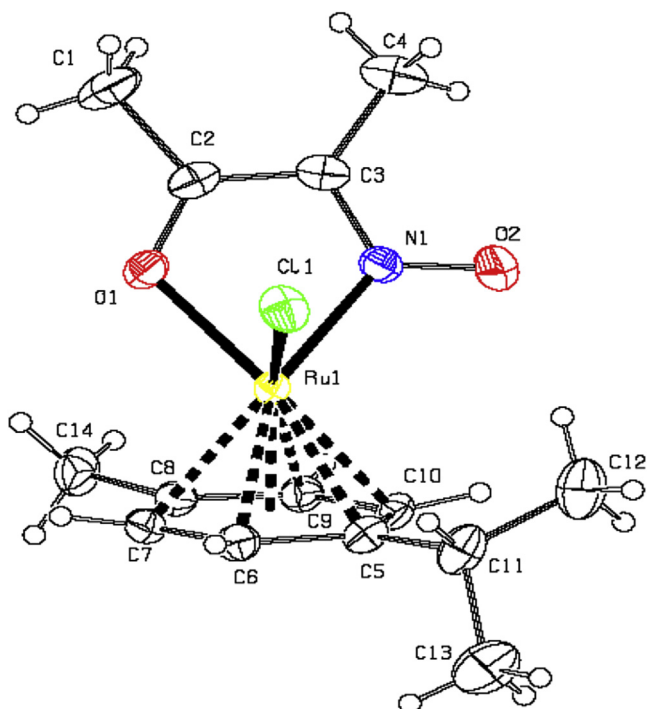


Fig. 1. Molecular structure of compound **1** showing the labeling scheme of the non-H atoms. Selected bond lengths (Å) and angles (°): Ru(1)–Cl(1) 2.3970(6), Ru(1)–O(1) 2.0694(14), Ru(1)–N(1) 2.0414(17), N(1)–O(2) 1.256(2), N(1)–C(3) 1.339(3), C(2)–C(3) 1.411(4), Ru–C_{cym(max)} 2.2207(19), Ru–C_{cym(min)} 2.1836(18), Cl(1)–Ru(1)–O(1) 85.25(5), Cl(1)–Ru(1)–N(1) 84.69(5), N(1)–Ru(1)–O(1) 77.13(7), Cl(1)–Ru(1)–centroid_{cym} 127.53, O(1)–Ru(1)–centroid_{cym} 130.68, N(1)–Ru(1)–centroid_{cym} 133.37.

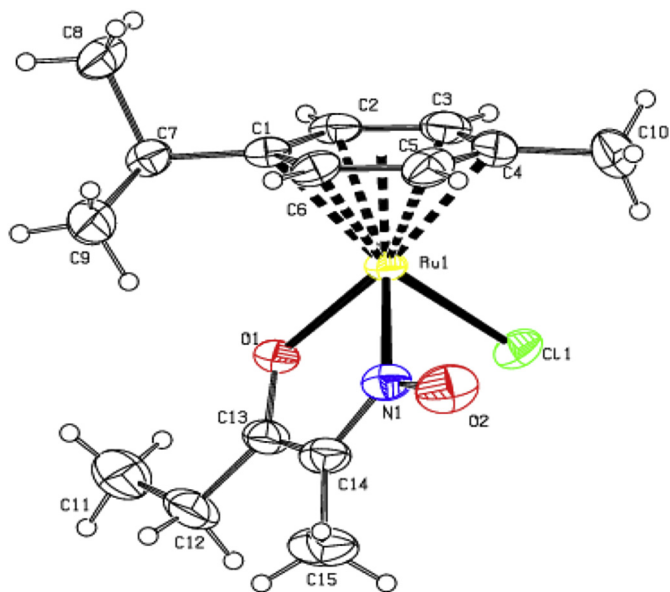


Fig. 2. Molecular structure of compound **3** showing the labeling scheme of the non-H atoms. Selected bond lengths (Å) and angles (°): Ru(1)–Cl(1) 2.3970(6), Ru(1)–O(1) 2.071(2), Ru(1)–N(1) 2.034(3), N(1)–O(2) 1.282(5), N(1)–C(14) 1.332(5), C(13)–C(14) 1.402(6), Ru–C_{cym(max)} 2.205(4), Ru–C_{cym(min)} 2.149(4), Cl(1)–Ru(1)–O(1) 86.08(7), Cl(1)–Ru(1)–N(1) 85.85(9), N(1)–Ru(1)–O(1) 76.87(13), Cl(1)–Ru(1)–centroid_{cym} 127.55, O(1)–Ru(1)–centroid_{cym} 131.39, N(1)–Ru(1)–centroid_{cym} 131.44.

determined owing to compound precipitation) and two ligands (**HL**¹ and **HL**⁹) were screened for preliminary *in vitro* antitumor activity with cisplatin as a positive control. The *in vitro* cytotoxicity

has been tested on various human tumor cell lines: human breast cancer cell lines (MCF-7), human cervical cancer cell lines (Hela), human hepatoma cell lines (HepG2).

As shown in Table 1, complexes **1–9** exhibit weak cytotoxicity against three human cancer cell lines (MCF-7, Hela and HepG2) with IC₅₀ values above 57.9 μM, which are much higher than that of cisplatin with IC₅₀ values of 4.9–11.3 μM.

In comparison with the ligands (**HL**¹ and **HL**⁹), almost all of ruthenium(II)-cymene complexes show enhanced activities than that of the ligands, confirming the beneficial effect of complexation to arene ruthenium units.

Among **1, 2, 3, 4** and **7** with different straight-chain α-ketoximes ligands, **1** with the shortest length of carbon chain showed stronger cytotoxicity with the IC₅₀ values of 59.9–100.9 μM (the order of activities follows **1** > **2** > **7** > **3** > **4**). For **5, 8** and **9** with different aromatic rings ligands, they are weaker than **1** in anti-proliferative activity, indicating the higher importance of alkyl substituent of α-diketone monoxime ligands.

In addition, for three human cancer cell lines treated in experiment, the ruthenium(II)-cymene-ketoxime compounds are relatively more sensitive to Hela cells.

2.5. Cell apoptosis analysis by flow cytometry

To gain more insights relative to the antitumor mechanism, compounds **1, 2** and **5** with relative stronger activities and ligand **HL**¹ were chosen for further experiments. Since Hela cells appeared to be the more sensitive than the other tested cells, we carried out flow cytometry assays to determine the apoptosis level of Hela cells exposed to **1, 2** and **5**. The results of cell apoptosis analysis by flow cytometry were shown in Table 2 and Fig. 4.

We can see that the total apoptosis percentages of the positive control are 14.14, 90.46 and 91.08% at the concentration of 2.0, 100 and 200 μM, respectively, and nearly equal to the negative control (ca. 11.08%) at low concentrations, while the total apoptosis of cisplatin increased obviously. This indicates cisplatin induced Hela cells apoptosis in a dose-dependent manner.

For ligand **HL**¹, the total apoptosis percentages are always below 10.01% at low (2 μM) or high (200 μM) concentrations. Compared with the control group, these data show ligand **HL**¹ could not induce Hela cancer cell apoptosis, which correlate with its weak cytotoxicity.

Complexes **1, 2** and **5**, at low concentrations (2.0 μM) do not induce apoptosis in Hela cells. With the increase of the concentrations of **1, 2** and **5**, the apoptosis rates increased obviously. The total apoptosis percentages are up to 85.47 and 91.54% for **1, 81.51** and 94.55% for **2** and 83.10 and 88.24% for **5** at the concentrations of 100 and 200 μM, respectively, which are higher than the negative control, but comparable with the positive control. Moreover, by comparing the percentages of early apoptosis (Q4) and late apoptosis (Q2) of cisplatin, we noticed that cisplatin can induce both early apoptosis and late apoptosis of Hela cells, which is different from the ruthenium-cymene-ketoxime complexes.

From the data of the apoptosis detection of **1, 2** and **5** (see Table 2), we also can see that the percentages of early apoptosis (Q4) are bigger than that of late apoptosis and necrotic cell (Q2). Moreover, with the increasing concentrations of compounds, there have been marked increases in the ratio of early apoptosis. The results suggest that cell death might be mainly by means of early apoptosis at high concentrations of the complexes, which is beneficial for optimal antitumor agents.

2.6. Cell cycle analysis by flow cytometry

The cell cycle is a series of events leading to cell division and

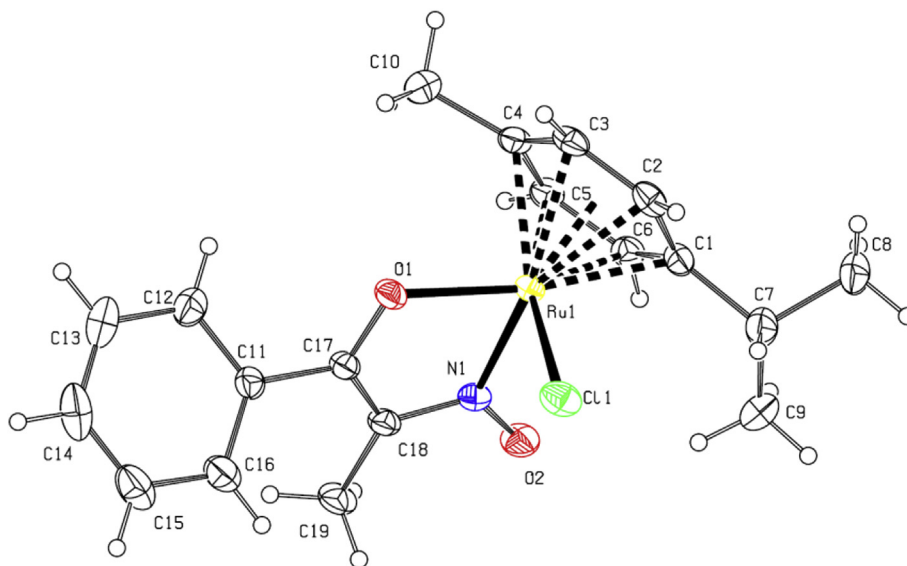


Fig. 3. Molecular structure of compound **5** showing the labeling scheme of the non-H atoms. Selected bond lengths (Å) and angles (°): Ru(1)–Cl(1) 2.3984(6), Ru(1)–O(1) 2.0739(15), Ru(1)–N(1) 2.0261(16), N(1)–O(2) 1.256(2), N(1)–C(18) 1.350(3), C(17)–C(18) 1.408(3), Ru–C_{cym(max)} 2.2415(18), Ru–C_{cym(min)} 2.171(2), Cl(1)–Ru(1)–O(1) 84.67(5), Cl(1)–Ru(1)–N(1) 88.22(5), N(1)–Ru(1)–O(1) 77.10(6), Cl(1)–Ru(1)–centroid_{cym} 127.47, O(1)–Ru(1)–centroid_{cym} 132.08, N(1)–Ru(1)–centroid_{cym} 129.99.

Table 1

Cytotoxicity of eight ruthenium(II) compounds and two ligands (**HL**¹ and **HL**⁹) against three human cancer cell lines (MCF-7, HeLa and HepG2). Data were presented as mean ± S.D. of three independent experiments.

Compounds	IC ₅₀ (μM)		
	MCF-7	HeLa	HepG2
1	90.0 ± 8.8	59.9 ± 5.1	100.9 ± 14.7
2	119.4 ± 24.5	57.9 ± 6.9	130.8 ± 83.9
3	264.0 ± 15.9	171.9 ± 14.7	337.2 ± 28.0
4	359.3 ± 30.4	341.9 ± 24.2	500.1 ± 60.3
5	126.8 ± 11.7	78.8 ± 5.5	76.8 ± 6.2
7	263.3 ± 20.2	159.2 ± 16.8	327.2 ± 25.1
8	282.5 ± 34.0	99.7 ± 18.8	283.9 ± 33.2
9	285.2 ± 34.0	122.4 ± 8.7	132.8 ± 12.8
HL ¹	>1000	>1000	>1000
HL ⁹	436.3 ± 53.4	162.5 ± 19.5	190.9 ± 24.6
cisplatin	11.3 ± 1.9	4.9 ± 0.6	3.1 ± 0.4

replication [30]. In an attempt to study the mechanism of cell apoptosis, flow cytometry analysis was performed to examine the

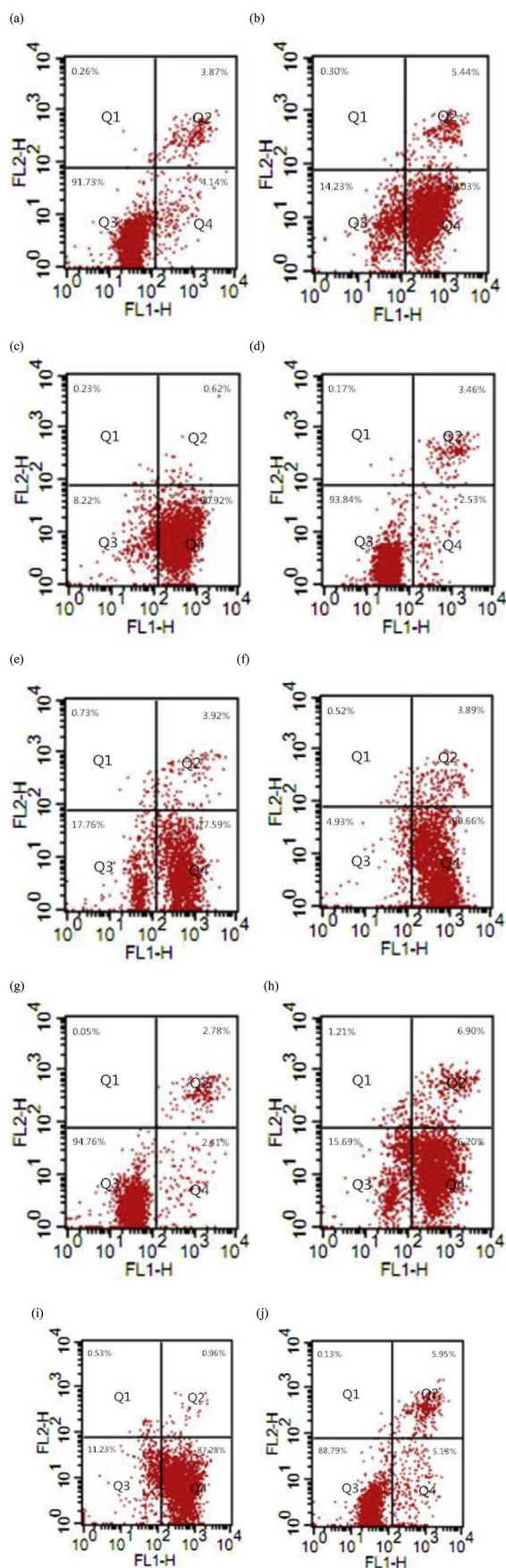
cell cycle progression in propidium-iodide-stained cells after HeLa cells were incubated with 100 μM of complexes **1**, **2** and **5** for 48 h. The results of cell cycle analysis by flow cytometry are shown in Fig. 5.

In the control, the percentage in the cells at G₂/M phase is 10.68%, whereas the percentages in the cells at G₂/M phase are 43.71, 37.79 and 30.43% after HeLa cells were treated with complexes **1**, **2** and **5** for 48 h, respectively. Comparing with the control, an enhancement of 33.03% for **1**, 27.11% for **2** and 19.75% for **5** in the cells at G₂/M phase was found, which was accompanied a reduction in the G₀/G₁ phase. Obviously, complexes **1**, **2** and **5** showed similar inhibitory effects in HeLa cells on the cell cycle arrest. These data suggest that complexes **1**, **2** and **5** altered cell cycle progression through inhibiting the cell growth of HeLa cells at G₂/M phase. Cisplatin is a cell cycle non-specific drug. At the same concentration, cisplatin blocked HeLa cells in S phase strongly, but blocked same cells in G₂-M phase slightly [31]. Therefore, the cycle arrest of compound **1**, **2** and **5** is different from cisplatin, but shows a similar behavior with NAMI-A [36].

Table 2

Percentages of apoptosis of compounds (**1**, **2**, **5** and **HL**¹) against HeLa cells in different concentrations with cisplatin as positive control.

Compd.	Conc. (μM)	Q ₂ (late apoptosis and necrotic cell, %)	Q ₄ (early apoptosis, %)	Q ₂ +Q ₄ (Total percentage)
Control	–	5.95	5.13	11.08
1	200	0.62	90.92	91.54
	100	5.44	80.03	85.47
	2	3.87	4.14	8.03
2	200	3.89	90.66	94.55
	100	3.92	77.59	81.51
	2	3.46	2.53	5.99
5	200	0.96	87.28	88.24
	100	6.90	76.20	83.10
	2	2.78	2.41	5.19
HL ¹	200	3.65	3.91	7.56
	100	4.04	4.77	8.83
	2	4.76	5.25	10.01
Cisplatin	200	34.56	56.52	91.08
	100	28.53	61.93	90.46
	2	5.54	8.60	14.14



2.7. Scratch wound healing assay

Cell has a natural tendency for migration that is a vital process in the growth and safeguarding of tissue functions [32]. The cell migration is very essential during embryogenesis, wound healing, development of immune response, etc. It also takes place in several diseases, especially in cancer, leading to invasion and metastasis [33]. Therefore, we have investigated the effect of **1–9** on cancer cell migration in highly metastatic (more migration rate) HepG2 cell line through scratch wound healing assay.

The experimental results show that compounds **2–8** seem no obvious anti-migration effect. We observed the scratch assay images in HepG2 treated with **1** and **9** at 150 μM with time. The untreated control cells migrated rapidly in a time dependent fashion due to metastatic property, while cells treated with **1** or **9** migrated in a slow rate. The wound area almost remained unchanged in cells incubated with **9**, further indicating its good anti-migration effects. Compared with untreated control, the wound closure of **1** was much lower than that of **9** in 6 h of incubation. Whereas in 24 h, compound **9** showed the lowest wound closure (Fig. 6) [34]. This result indicates that these complexes may have great potential to be anti-metastatic through the inhibition of cancer cells migration.

2.8. Invasion assay

Invasive ability was measured in a transwell cell culture chamber according to the method of Albini [35], and the images of invasion assay are shown in Fig. 7.

From the images of the transwell assay, we observed that there were a lot of HepG2 cells in the blank group (control), while the HepG2 cells treated with **1** or **9** were much less than that of control group, indicating that **1** and **9** are able to inhibit the invasion of HepG2 cells, and the anti-invasive ability of **9** is stronger than that of **1**.

2.9. Effects of expression of E-cadherin and Vimentin

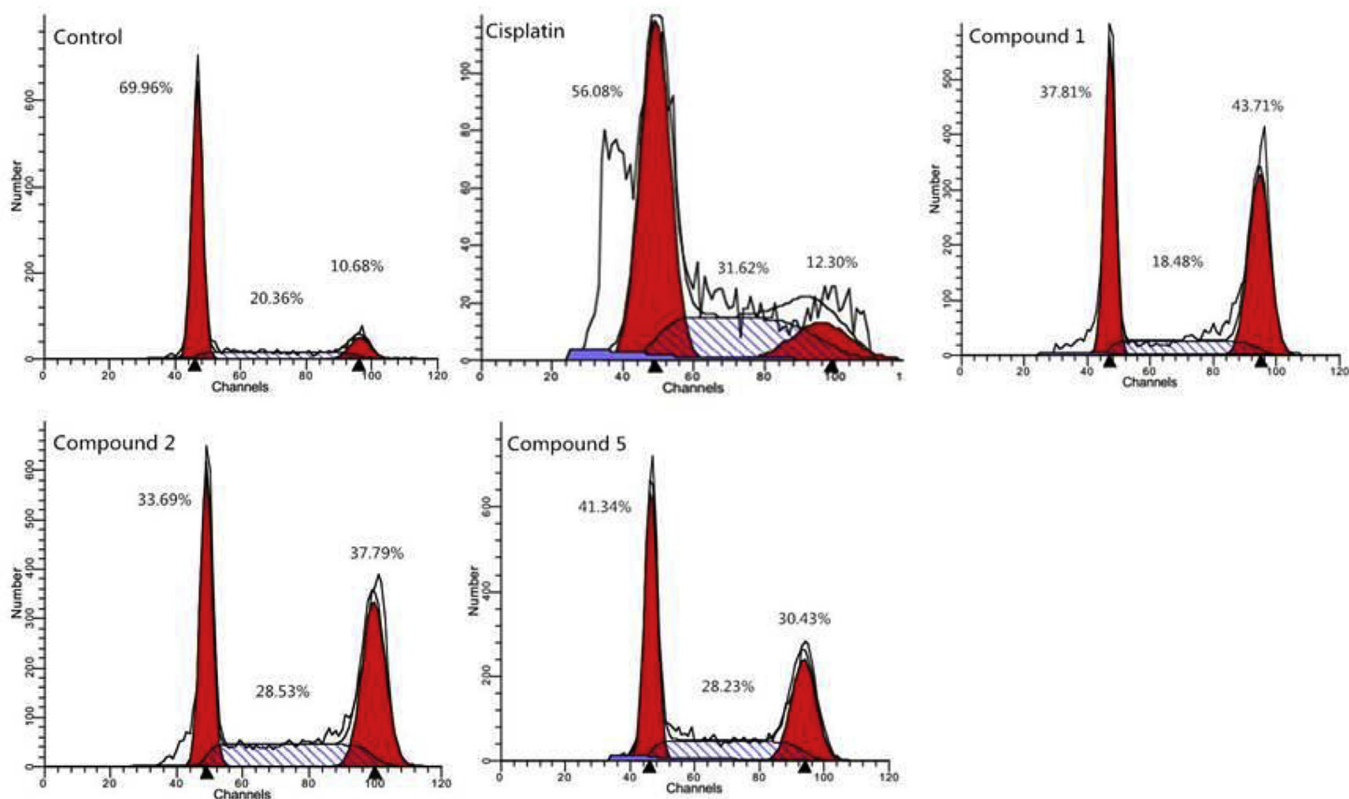
Recent experimental evidence suggests when lack of *in vitro* cytotoxicity is associated to inhibition of matrigel invasion, it may predict *in vivo*-selective antimetastasis activity of ruthenium complexes [36]. In order to understand the molecular targeting and mechanism of action of ruthenium(II)-cymene compounds, according to the invasion assay results, we choose compound **9**, the anti-metastasis compound with low cytotoxicity, to study the preliminary anti-metastasis action by Western blotting.

The activation of anti-Bcl-2 E-cadherin, anti-Bcl-2 vimentin, anti-cyclin-D1 and anti-cyclin-E1 antibody was assayed by western blot analysis. As shown in Fig. 8, we can see the high expression of both cyclin D1 and cyclin E1 in control group. After the treatment of HepG2 cells with different concentrations of compound **9**, the expression levels of cyclin-D1 and cyclin-E1 decreased significantly, indicating that compound **9** can block cells in the G1 phase, down-regulate the expression of cyclin-D1 and cyclin-E1, and inhibit cyclin-D1/cyclin-E1 *in vitro*. Thus the expression of both cyclin-D1 and cyclin-E1 is correlated with the antiproliferative effect of compound **9**.

E-cadherin is an important cell adhesion molecule cadherin family member, which play an important role in the maintenance of

Fig. 4. Apoptosis detection HeLa cells using FITC-PI assay after 48 h. The total percentage of apoptotic cells was considered as Q2 + Q4. Plot presents the fluorescence data of propidium iodide (PI) and Annexin V fluorescence in corresponding to (a) **1**, 2 μM , (b) **1**, 100 μM , (c) **1**, 200 μM , (d) **2**, 2 μM , (e) **2**, 100 μM , (f) **2**, 200 μM , (g) **5**, 2 μM (h) **5**, 100 μM , (i) **5**, 200 μM , (j) control.

(A)



(B)

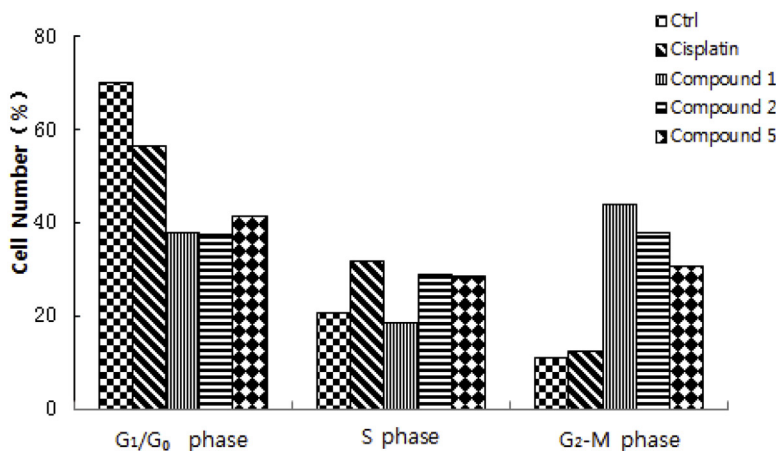


Fig. 5. Cell cycle distribution of HeLa cells after the treatment with 100 μ M of compounds (A). Data analysis of cell cycle arrest (B).

cell adhesion, cell polarity and cell communication [22]. Vimentin is a key member of intermediate filament protein family, which is known to play a significant role in the maintenance of cell integrity and against external stress injury [37]. EMT is one of the main mechanisms of promoting tumor invasion and metastasis [37,38]. E-cadherin and Vimentin are important markers of EMT. As shown in Fig. 8, we can observe the expression of Vimentin decreased slightly, whereas the expression of E-cadherin increased obviously. The increased expression of E-cadherin and reduced expression of Vimentin illustrate the potent ability of compound 9 in anti-tumor

invasion and metastasis. These observations also suggest that cyclin-D1, cyclin-E1 and vimentin may be the cellular targets of these ruthenium complexes with α -dicarbonylmonoximes.

3. Conclusions

In this work we have reported the synthesis of a series of new ruthenium(II)-cymene complexes with substituted α -dicarbonylmonoxime ligands (1–9). All compounds were subjected to characterization by elemental analysis, IR, ¹H NMR, ¹³C NMR

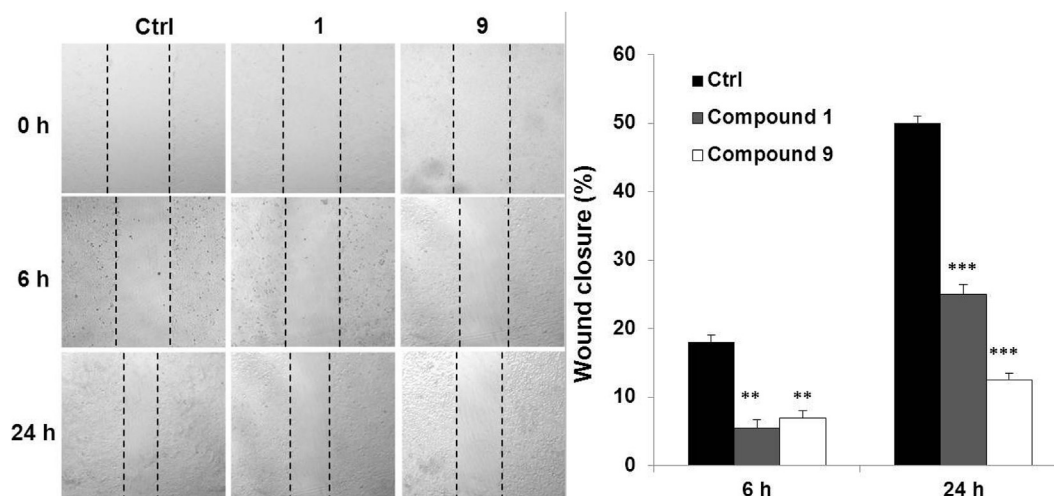


Fig. 6. Images of scratch assay in HepG2 cells treated with **1** or **9** at 150 μ M at 0 h, 6 h and 24 h (culture medium as control) (left). Wound closure (%) was quantified by calculating the change of wound width (right). Data were presented as mean \pm S.D. of three independent experiments. Statistical analyses were performed using Student's *t*-test. ***P* < 0.01 and ****P* < 0.001.

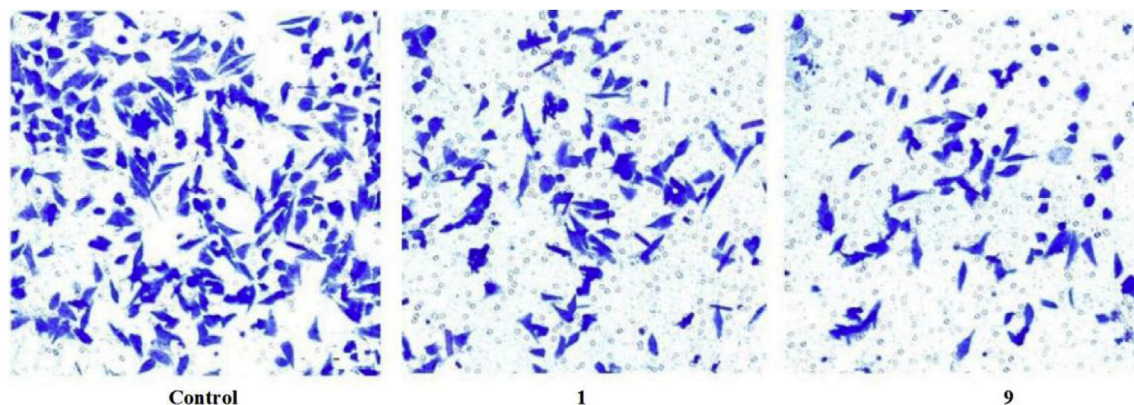


Fig. 7. Images of transwell assay in HepG2 cells treated with **1** or **9** at 100 μ M at 24 h (culture medium as control).

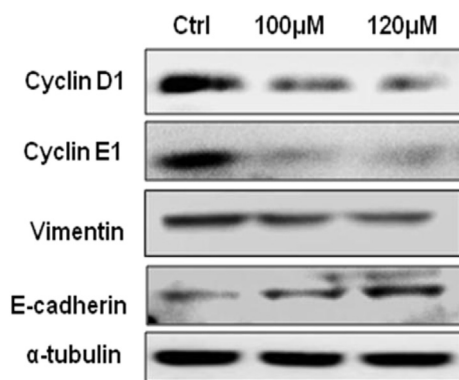


Fig. 8. The expression of anti-Bcl-2 E-cadherin, anti-Bcl-2 Vimentin, anti-Cyclin-D1 and anti-Cyclin-E1 antibody were assayed by western blot analysis, after the treatment of HepG2 cells with compound **9** at 100 μ M and 120 μ M.

spectroscopies, and in three cases by single crystal X-ray diffraction analysis. The X-ray structure analyses revealed a pseudo-octahedral 'piano-stool' configuration for the metals with bidentate coordination through oxime-N and α -ketone-O, forming a nearly planar five-membered metallocycle. Eight complexes were tested for their

cytotoxicity against three different human cancer cells (MCF-7, HeLa and HepG2). Relative to cisplatin, these ruthenium(II)-cymene complexes are found to be lack of *in vitro* cytotoxicity.

Apoptosis and cell cycle analysis showed that the selected three ruthenium compounds induced a similar accumulation of HeLa cells in the G2-M phase, while cisplatin is known to induce initial S-phase arrest as a DNA replication blockade. This shows that the ruthenium(II) complexes can have an action mechanism different from that of Pt drugs. For this type of relatively non-cytotoxic compounds [Ru(η^6 -cymene)(L)Cl] (L = α -dicarbonylmonoxime derivatives), the main targets should not be DNA.

In addition, scratch wound healing assay and transwell test showed that **1** and **9** could inhibit tumor cells migration and invasion of matrigel, indicating that these complexes may have great anti-metastatic potential. Protein level analysis shows that the anti-metastasis action is associated with the increasing expression of E-cadherin and reducing expression of Vimentin.

In summary, our study provides a novel type of ruthenium(II) therapeutic agents that aim to block cancer cell migration and invasion without exerting cell toxicity. Both **1** and **9** have shown to have some similar antitumor effects to NAMI-A, namely low cytotoxicity *in vitro*, and remarkable anti-invasion and metastasis properties. The preliminary anti-migration activity of these

compounds may be a result of abnormal expression of E-cadherin and vimentin. Further studies deserve to be undertaken which may be helpful for the design of new ruthenium-based anticancer agents.

4. Experimental section

4.1. Materials and physical measurements

RuCl₃·3H₂O and 1,2-indanedione (HL⁸) were purchased from Aldrich. [Ru(η⁶-p-cymene)Cl₂]₂ [39] and the ligands 2,3-pentanedione-2-oxime (HL³), 2,3-hexanedione-2-oxime (HL⁴), α-benzil monoxime (HL⁶), 3,4-hexanedione-3-oxime (HL⁷) and acenaphthenequinone monooxime (HL⁹) were synthesized using literature methods [40,41]. The ligands diacetylmonoxime (HL¹), (Z)-2-oxopropanal oxime (HL²), 1-phenyl-1,2-propanedione-2-oxime (HL⁵) and all other chemicals were obtained from Sino-pharm Chemical Reagent Co. Ltd., China and were used as received. All biological materials were purchased from Wuhan Goodti meBio–Technology Co. Ltd., China. Elemental analyses were performed with a Perkin-Elmer 2400 analyzer, series II. IR spectra were recorded from 4000 to 400 cm⁻¹ with a Bruker Vertex 70 FT–IR spectrophotometer on KBr pellets; only significant bands are cited in the text. NMR spectra were recorded with a Bruker AM-400 spectrometer. ¹H and ¹³C chemical shifts are reported relative to tetramethylsilane.

4.2. Synthesis of the [Ru(η⁶-p-cymene)(L)Cl] complexes (1–9)

4.2.1. Synthesis of [Ru(η⁶-p-cymene)(L¹)Cl] (1)

244.8 mg (0.4 mmol) [Ru(η⁶-p-cymene)Cl₂]₂ was added to a methanol (15 mL) solution of 80.9 mg (0.8 mmol) diacetyl monoxime (HL¹), and the mixture was stirred at room temperature for 1.5 h. The solvent was removed under reduced pressure, and the crude product was purified by silica gel column chromatography (V_{chloroform}: V_{acetone} = 10:1). The solid was then recrystallized from dichloromethane–n-hexane. Purple crystals were obtained. Yield: 51.7%. M.p.: 142.0–143.7 °C. Anal. Calcd. for C₁₄H₂₀ClNO₂Ru: C 45.34, H 5.44, N 3.78. Found: C 45.71, H 5.24, N 3.85. IR (KBr): ν = 1637 (C=O/N=C), 1529, 1330, 977 (N=O/N–O), 519 (Ru–N), 478 (Ru–O) cm⁻¹. ¹H NMR (CDCl₃): δ = 1.24 (d, 3H, CH₃C₆H₄CH(CH₃)₂, J = 6.8 Hz), 1.25 (d, 3H, CH₃C₆H₄CH(CH₃)₂, J = 6.8 Hz), 1.90 (s, 3H, N=C–CH₃), 2.26 (s, 3H, CH₃C₆H₄CH(CH₃)₂), 2.35 (s, 3H, O=C–CH₃), 2.85–2.92 (m, 1H, CH₃C₆H₄CH(CH₃)₂), δ = 5.30 (d, 1H, –C₆H₄–, J = 6.0 Hz), 5.33 (d, 1H, –C₆H₄–, J = 6.0 Hz), 5.49 (d, 1H, –C₆H₄–, J = 6.0 Hz), 5.52 (d, 1H, –C₆H₄–, J = 6.0 Hz) ppm. ¹³C NMR (CDCl₃): δ = 11.2 (N=C–CH₃), 18.5 (CH₃C₆H₄CH(CH₃)₂), 22.0 (O=C–CH₃), 22.4, 24.2 (CH₃C₆H₄CH(CH₃)₂), 30.8 (CH₃C₆H₄CH(CH₃)₂), 83.2, 84.0, 84.5, 86.4, 100.3, 103.6 (CH₃C₆H₄CH(CH₃)₂), 152.8 (N=C–CH₃), 201.5 (O=C–CH₃) ppm.

4.2.2. Synthesis of [Ru(η⁶-p-cymene)(L²)Cl] (2)

Compound **2** was prepared analogously by following the method and conditions described for **1** but using HL² (1.0 mmol) and [Ru(η⁶-p-cymene)Cl₂]₂ (0.5 mmol). Orange-red solids were obtained. Yield: 31.3%. M.p.: 134.1–135 °C. Anal. Calcd. for C₁₃H₁₈ClNO₂Ru: C 43.76, H 5.08, N 3.93. Found: C 44.11, H 4.92, N 4.06. IR (KBr): ν = 1619 (C=O/N=C), 1513, 1358, 981 (N=O/N–O), 483 (Ru–N), 450 (Ru–O) cm⁻¹. ¹H NMR (CDCl₃): δ = 1.24 (d, 3H, CH₃C₆H₄CH(CH₃)₂, J = 7.2 Hz), 1.26 (d, 3H, CH₃C₆H₄CH(CH₃)₂, J = 7.2 Hz), 2.26 (s, 3H, O=C–CH₃), 2.28 (s, 3H, CH₃C₆H₄CH(CH₃)₂), 2.84–2.91 (m, 1H, CH₃C₆H₄CH(CH₃)₂), 5.28 (d, 1H, –C₆H₄–, J = 6.0 Hz), 5.37 (d, 1H, –C₆H₄–, J = 6.0 Hz), 5.50 (d, 1H, –C₆H₄–, J = 6.0 Hz), 5.53 (d, 1H, –C₆H₄–, J = 6.0 Hz), 7.43 (s, 1H, O=N=C–H) ppm. ¹³C NMR (CDCl₃): δ = 18.5 (CH₃C₆H₄CH(CH₃)₂), 22.0 (O=C–

CH₃), 22.4, 23.2 (CH₃C₆H₄CH(CH₃)₂), 30.9 (CH₃C₆H₄CH(CH₃)₂), 83.0, 84.0, 84.8, 86.5, 100.9, 104.3 (CH₃C₆H₄CH(CH₃)₂), 145.0 (O=N=C–H), 202.0 (O=C–CH₃) ppm.

4.2.3. Synthesis of [Ru(η⁶-p-cymene)(L³)Cl] (3)

Compound **3** was prepared analogously by following the method and conditions described for **1** but using HL³ (1.0 mmol) and [Ru(η⁶-p-cymene)Cl₂]₂ (0.5 mmol). Dark red crystals were obtained. Yield: 35.6%. M.p.: 107.8–109.4 °C. Anal. Calcd. for C₁₅H₂₂ClNO₂Ru: C 46.81, H 5.76, N 3.64. Found: C 47.26, H 5.53, N 3.69. IR (KBr): ν = 1629 (C=O/N=C), 1524, 1340, 994 (N=O/N–O), 519 (Ru–N), 465 (Ru–O) cm⁻¹. ¹H NMR (CDCl₃): δ = 1.20 (t, 3H, CH₃CH₂, J = 7.2 Hz), 1.24 (d, 3H, CH₃C₆H₄CH(CH₃)₂, J = 7.2 Hz), 1.26 (d, 6H, CH₃C₆H₄CH(CH₃)₂, J = 7.2 Hz), 1.90 (s, 3H, N=C–CH₃), 2.27 (s, 3H, CH₃C₆H₄CH(CH₃)₂), 2.60–2.67 (m, 2H, O=C–CH₂CH₃), 2.84–2.91 (m, 1H, CH₃C₆H₄CH(CH₃)₂), δ = 5.33 (m, 2H, –C₆H₄–), 5.47 (m, 1H, –C₆H₄–), 5.55 (m, 1H, –C₆H₄–) ppm. ¹³C NMR (CDCl₃): δ = 9.4 (CH₃CH₂C=O), 10.8 (CH₃C=N), 18.5 (CH₃C₆H₄CH(CH₃)₂), 22.0, 22.4 (CH₃C₆H₄CH(CH₃)₂), 30.0 (O=C–CH₂CH₃), 30.9 (CH₃C₆H₄CH(CH₃)₂), 83.7, 84.3, 84.8, 86.0, 99.5, 103.3 (CH₃C₆H₄CH(CH₃)₂), 152.3 (O=N=C–CH₃), 205.1 (O=C–CH₂CH₃) ppm.

4.2.4. Synthesis of [Ru(η⁶-p-cymene)(L⁴)Cl] (4)

Compound **4** was prepared analogously by following the method and conditions described for **1** but using HL⁴ (1.0 mmol) and [Ru(η⁶-p-cymene)Cl₂]₂ (0.5 mmol). Red solids were obtained. Yield: 24.3%. M.p.: 77.7–79.3 °C. Anal. Calcd. for C₁₆H₂₄ClNO₂Ru: C 48.18, H 6.06, N 3.51. Found: C 48.58, H 5.73, N 3.59. IR (KBr): ν = 1627 (C=O/N=C), 1524, 1350, 943 (N=O/N–O), 525 (Ru–N), 473 (Ru–O) cm⁻¹. ¹H NMR (CDCl₃): δ = 0.92 (t, 3H, CH₃CH₂C=N, J = 7.6 Hz), 1.17–1.23 (m, 9H, CH₃CH₂C=O, CH₃C₆H₄CH(CH₃)₂), 2.23–2.30 (m, 4H, N=C–CH₃, CH₃CH₂C=N), 2.37–2.44 (m, 1H, CH₃CH₂C=N), 2.56–2.62 (m, 2H, O=C–CH₂CH₃), 2.80–2.86 (m, 1H, CH₃C₆H₄CH(CH₃)₂), δ = 5.26 (d, 1H, –C₆H₄–, J = 6.0 Hz), 5.34 (d, 1H, –C₆H₄–, J = 6.0 Hz), 5.50 (d, 1H, –C₆H₄–, J = 6.0 Hz), 5.53 (d, 1H, –C₆H₄–, J = 6.0 Hz) ppm. ¹³C NMR (CDCl₃): δ = 9.7 (CH₃CH₂C=N), 11.0 (CH₃CH₂C=O), 18.4 (CH₃CH₂C=N), 18.5 (CH₃C₆H₄CH(CH₃)₂), 21.9, 22.4 (CH₃C₆H₄CH(CH₃)₂), 30.0 (O=C–CH₂CH₃), 30.9 (CH₃C₆H₄CH(CH₃)₂), 83.1, 84.1, 84.8, 86.3, 100.4, 103.1 (CH₃C₆H₄CH(CH₃)₂), 158.1 (O=N=CH₂CH₃), 205.1 (O=C–CH₂CH₃) ppm.

4.2.5. Synthesis of [Ru(η⁶-p-cymene)(L⁵)Cl] (5)

Compound **5** was prepared analogously by following the method and conditions described for **1** but using HL⁵ (1.0 mmol) and [Ru(η⁶-p-cymene)Cl₂]₂ (0.5 mmol). Purple crystals were obtained. Yield: 27.0%. M.p.: 155.8–157.4 °C. Anal. Calcd. for C₁₉H₂₂ClNO₂Ru: C 52.71, H 5.12, N 3.24. Found: C 53.13, H 4.94, N 3.35. IR (KBr): ν = 1635 (C=O/N=C), 1521, 1341, 971 (N=O/N–O), 513 (Ru–N), 451 (Ru–O) cm⁻¹. ¹H NMR (DMSO-d₆): δ = 1.19 (d, 3H, CH₃C₆H₄CH(CH₃)₂, J = 6.8 Hz), 1.20 (d, 3H, CH₃C₆H₄CH(CH₃)₂, J = 6.8 Hz), 1.90 (s, 3H, O=C–CH₃), 2.17 (s, 3H, CH₃C₆H₄CH(CH₃)₂), 2.75–2.80 (m, 1H, CH₃C₆H₄CH(CH₃)₂), 5.52 (d, 1H, –C₆H₄–, J = 6.0 Hz), 5.56 (d, 1H, –C₆H₄–, J = 6.0 Hz), 5.69 (d, 1H, –C₆H₄–, J = 6.0 Hz), 5.81 (d, 1H, –C₆H₄–, J = 6.0 Hz), 7.51–7.64 (m, 5H, Ar–H) ppm. ¹³C NMR (DMSO-d₆): δ = 18.4 (CH₃C₆H₄CH(CH₃)₂), 22.0 (O=C–CH₃), 22.1, 22.4 (CH₃C₆H₄CH(CH₃)₂), 30.9 (CH₃C₆H₄CH(CH₃)₂), 83.8, 84.7, 85.7, 87.2, 101.0, 103.2 (CH₃C₆H₄CH(CH₃)₂), 126.5, 128.5, 129.0, 129.3, 132.3, 136.0 (C₆H₅–C=N), 152.1 (O=N=C–C₆H₅), 195.2 (O=C–CH₃) ppm.

4.2.6. Synthesis of [Ru(η⁶-p-cymene)(L⁶)Cl] (6)

Compound **6** was prepared analogously by following the method and conditions described for **1** but using HL⁶ (1.0 mmol)

and $[\text{Ru}(\eta^6\text{-}p\text{-cymene})\text{Cl}_2]_2$ (0.5 mmol). Purple crystals were obtained. Yield: 28.6%. M.p.: 192.6–194.2 °C. Anal. Calcd. for $\text{C}_{24}\text{H}_{24}\text{ClNO}_2\text{Ru}$: C 58.24, H 4.89, N 2.83. Found: C 58.78, H 4.69, N 2.93. IR (KBr): $\nu = 1638$ (C=O/N=C), 1512, 1373, 999 (N=O/N=O), 505 (Ru–N), 479 (Ru–O) cm^{-1} . ^1H NMR (CDCl_3): $\delta = 1.32$ (d, 3H, $\text{CH}_3\text{C}_6\text{H}_4\text{CH}(\text{CH}_3)_2$, $J = 6.8$ Hz), 1.34 (d, 3H, $\text{CH}_3\text{C}_6\text{H}_4\text{CH}(\text{CH}_3)_2$, $J = 6.8$ Hz), 2.36 (s, 3H, $\text{CH}_3\text{C}_6\text{H}_4\text{CH}(\text{CH}_3)_2$), 2.94–3.02 (m, 1H, $\text{CH}_3\text{C}_6\text{H}_4\text{CH}(\text{CH}_3)_2$), 5.42 (d, 1H, $-\text{C}_6\text{H}_4-$, $J = 6.0$ Hz), 5.47 (d, 1H, $-\text{C}_6\text{H}_4-$, $J = 6.0$ Hz), 5.57 (d, 1H, $-\text{C}_6\text{H}_4-$, $J = 6.0$ Hz), 5.67 (d, 1H, $-\text{C}_6\text{H}_4-$, $J = 6.0$ Hz), $\delta = 7.06$ –7.38 (m, 10H, Ar–H) ppm. ^{13}C NMR ($\text{DMSO-}d^6$): $\delta = 18.5$ ($\text{CH}_3\text{C}_6\text{H}_4\text{CH}(\text{CH}_3)_2$), 22.1, 22.4 ($\text{CH}_3\text{C}_6\text{H}_4\text{CH}(\text{CH}_3)_2$), 40.0 ($\text{CH}_3\text{C}_6\text{H}_4\text{CH}(\text{CH}_3)_2$), 83.9, 85.2, 85.9, 87.7, 102.0, 103.5 ($\text{CH}_3\text{C}_6\text{H}_4\text{CH}(\text{CH}_3)_2$), 128.6, 128.76, 129.1, 130.6, 131.7, 132.3, 135.8 ($-\text{C}_6\text{H}_5$), 155.7 (N=C– C_6H_5), 193.7 (O=C– C_6H_5) ppm.

4.2.7. Synthesis of $[\text{Ru}(\eta^6\text{-}p\text{-cymene})(\text{L}^7)\text{Cl}]$ (**7**)

Compound **7** was prepared analogously by following the method and conditions described for **1** but using HL^7 (1.0 mmol) and $[\text{Ru}(\eta^6\text{-}p\text{-cymene})\text{Cl}_2]_2$ (0.5 mmol). Purple solids were obtained. Yield: 47.4%. Anal. Calcd. for $\text{C}_{16}\text{H}_{24}\text{ClNO}_2\text{Ru}$: C 48.18, H 5.76, N 3.51. Found: C 48.32, H 5.69, N 3.67. IR (KBr): $\nu = 1622$ (C=O/N=C), 1525, 1337, 973 (N=O/N=O), 522 (Ru–N), 455 (Ru–O) cm^{-1} . ^1H NMR (CDCl_3): $\delta = 0.97$ (t, 3H, $\text{CH}_3\text{CH}_2\text{CH}_2$, $J = 7.6$ Hz), 1.24 (d, 3H, $\text{CH}_3\text{C}_6\text{H}_4\text{CH}(\text{CH}_3)_2$, $J = 7.2$ Hz), 1.26 (d, 3H, $\text{CH}_3\text{C}_6\text{H}_4\text{CH}(\text{CH}_3)_2$, $J = 7.2$ Hz), 1.69 (m, 2H, $\text{CH}_3\text{CH}_2\text{CH}_2$), 1.90 (s, 3H, N=C– CH_3), 2.26 (s, 3H, $\text{CH}_3\text{C}_6\text{H}_4\text{CH}(\text{CH}_3)_2$), 2.57–2.60 (t, 2H, O=C– CH_2CH_2), 2.83–2.90 (m, 1H, $\text{CH}_3\text{C}_6\text{H}_4\text{CH}(\text{CH}_3)_2$), $\delta = 5.33$ (t-like, 2H, $-\text{C}_6\text{H}_4-$), 5.47 (d, 1H, $-\text{C}_6\text{H}_4-$), 5.54 (d, 1H, $-\text{C}_6\text{H}_4-$) ppm. ^{13}C NMR (CDCl_3): $\delta = 11.0$ ($\text{CH}_3\text{CH}_2\text{CH}_2\text{C}=\text{O}$), 13.9 ($\text{CH}_3\text{C}=\text{N}$), 18.4 ($\text{CH}_3\text{C}_6\text{H}_4\text{CH}(\text{CH}_3)_2$), 19.0 ($\text{CH}_3\text{CH}_2\text{CH}_2\text{C}=\text{O}$), 21.9, 22.4 ($\text{CH}_3\text{C}_6\text{H}_4\text{CH}(\text{CH}_3)_2$), 30.9 ($\text{CH}_3\text{C}_6\text{H}_4\text{CH}(\text{CH}_3)_2$), 38.9 (O=C– $\text{CH}_2\text{CH}_2\text{CH}_3$), 83.6, 84.2, 84.6, 86.2, 99.8, 103.3 ($\text{CH}_3\text{C}_6\text{H}_4\text{CH}(\text{CH}_3)_2$), 152.8 (O=N=C– CH_3), 204.8 (O=C– CH_2CH_3) ppm.

4.2.8. Synthesis of $[\text{Ru}(\eta^6\text{-}p\text{-cymene})(\text{L}^8)\text{Cl}]$ (**8**)

Compound **8** was prepared analogously by following the method and conditions described for **1** but using HL^8 (1.0 mmol) and $[\text{Ru}(\eta^6\text{-}p\text{-cymene})\text{Cl}_2]_2$ (0.5 mmol). Black crystals were obtained. Yield: 22.6%. M.p.: 183.9–186.0 °C. Anal. Calcd. for $\text{C}_{19}\text{H}_{20}\text{ClNO}_2\text{Ru}$: C 52.96, H 4.68, N 3.25. Found: C 53.39, H 4.48, N 3.36. IR (KBr): $\nu = 1609$ (C=O/N=C), 1568, 1333, 967 (N=O/N=O), 513 (Ru–N), 449 (Ru–O) cm^{-1} . ^1H NMR (CDCl_3): $\delta = 1.17$ (d, 6H, $\text{CH}_3\text{C}_6\text{H}_4\text{CH}(\text{CH}_3)_2$, $J = 6.8$ Hz), 2.25 (s, 3H, $\text{CH}_3\text{C}_6\text{H}_4\text{CH}(\text{CH}_3)_2$), 2.79–2.86 (m, 1H, $\text{CH}_3\text{C}_6\text{H}_4\text{CH}(\text{CH}_3)_2$), 3.58 (dd, CH_2 –C=N, $J = 21.6$ Hz), 5.41, 5.43 (d, 1H, $-\text{C}_6\text{H}_4-$, $J = 6.0$ Hz), 7.06–7.12 (m, 4H, $-\text{C}_6\text{H}_4-$), 7.52 (d, 1H, Ar–H, $J = 7.2$ Hz), 7.53 (t-like, 1H, Ar–H, $J = 7.2$, 7.6 Hz), 7.61 (d, 1H, Ar–H, $J = 7.6$ Hz), 7.70 (t-like, 1H, Ar–H, $J = 6.4$, 7.6 Hz), 7.90 (d, 1H, Ar–H, $J = 7.6$ Hz) ppm. ^{13}C NMR ($\text{DMSO-}d^6$): $\delta = 21.0$ ($\text{CH}_3\text{C}_6\text{H}_4\text{CH}(\text{CH}_3)_2$), 24.4 ($\text{CH}_3\text{C}_6\text{H}_4\text{CH}(\text{CH}_3)_2$), 27.1 (CH_2 –C=N), 33.4 ($\text{CH}_3\text{C}_6\text{H}_4\text{CH}(\text{CH}_3)_2$), 126.5, 129.3, 135.0, 135.1 ($\text{CH}_3\text{C}_6\text{H}_4\text{CH}(\text{CH}_3)_2$), 123.9, 127.9, 128.3, 135.3, 145.8, 148.9 (Ar–H), 158.2 (N=C–Ar), 197.3 (O=C–Ar) ppm.

4.2.9. Synthesis of $[\text{Ru}(\eta^6\text{-}p\text{-cymene})(\text{L}^9)\text{Cl}]$ (**9**)

Compound **9** was prepared analogously by following the method and conditions described for **1** but using HL^9 (1.0 mmol) and $[\text{Ru}(\eta^6\text{-}p\text{-cymene})\text{Cl}_2]_2$ (0.5 mmol). Purple crystals were obtained. Yield: 28.6%. M.p. > 300 °C. Anal. Calcd. for $\text{C}_{22}\text{H}_{20}\text{ClNO}_2\text{Ru}$: C 56.59, H 4.32, N 3.00. Found: C 56.79, H 4.15, N 3.10. IR (KBr): $\nu = 1613$ (C=O), 1570 (C=N), 1374, 952 (N=O/N=O), 509 (Ru–N), 443 (Ru–O) cm^{-1} . ^1H NMR ($\text{DMSO-}d^6$): $\delta = 1.17$ (d, 6H, $\text{CH}_3\text{C}_6\text{H}_4\text{CH}(\text{CH}_3)_2$, $J = 6.8$ Hz), 2.25 (s, 3H, $\text{CH}_3\text{C}_6\text{H}_4\text{CH}(\text{CH}_3)_2$), 2.79–2.86 (m, 1H, $\text{CH}_3\text{C}_6\text{H}_4\text{CH}(\text{CH}_3)_2$), 7.06–7.12 (m, 4H, $\text{CH}_3\text{C}_6\text{H}_4\text{CH}(\text{CH}_3)_2$), 7.64–7.67 (dd, 1H, Ar–H, $J = 7.2$, 8.4 Hz), 7.84–7.88 (dd, 1H, Ar–H, $J = 7.2$, 8.0 Hz), 7.54–7.99 (m, 2H, Ar–H),

8.24 (d, 1H, Ar–H, $J = 7.2$ Hz), 8.34 (d, 1H, Ar–H, $J = 8.0$ Hz) ppm. ^{13}C NMR (CDCl_3): $\delta = 18.5$ ($\text{CH}_3\text{C}_6\text{H}_4\text{CH}(\text{CH}_3)_2$), 22.1, 22.4 ($\text{CH}_3\text{C}_6\text{H}_4\text{CH}(\text{CH}_3)_2$), 30.9 ($\text{CH}_3\text{C}_6\text{H}_4\text{CH}(\text{CH}_3)_2$), 82.2, 83.4, 83.9, 85.7, 99.3, 103.2 ($\text{CH}_3\text{C}_6\text{H}_4\text{CH}(\text{CH}_3)_2$), 120.9, 124.0, 125.7, 125.8, 127.5, 128.5, 128.6, 130.3, 133.2, 136.0 (Ar–H), 155.2 (N=C), 199.7 (O=C) ppm.

4.3. X-ray measurements

Suitable single crystals of compounds **1**, **3** and **5** were mounted in glass capillaries for X-ray structural analysis. Diffraction data were collected on a Bruker Smart APEX-II CCD diffractometer with Mo K α ($\lambda = 0.71076$ Å) radiation at room temperature. During the intensity data collection, no significant decay was observed. The intensities were collected for Lorentz-polarization effects and empirical absorption with the SADABS program. The structure was solved by direct methods using the SHELXL-97 program. All non-hydrogen atoms were found from the difference Fourier syntheses. The H atoms were included in calculated positions with isotropic thermal parameters related to those of the supporting carbon atoms but were not included in the refinement. All calculations were performed using the Bruker Smart program [42]. Crystallographic details are reported in Table 3.

4.4. Cytotoxic activity in vitro

The following cell lines were used for biological assays: human breast carcinoma cell line (MCF-7), cervical carcinoma cell line (Hela) and human liver hepatocellular carcinoma cell lines (HepG2). They were cultured with RPMI-1640 medium (Solarbio) containing 10% fetal bovine serum (Zhejiang Tianhang Biological Technology Co. Ltd., China), and placed at 37 °C in humidified incubators in an atmosphere of 5% CO_2 .

The complexes were dissolved in DMSO at a concentration of 20 mM as stock solution, and diluted in culture medium at concentrations of 1000, 400, 160, 64 and 25.6 μM as working solution. To avoid DMSO toxicity, the concentration of DMSO was less than 0.2% (v/v) in all experiments [43].

The cancer cells in exponential phase were digested with trypsin, and seeded into a 96-well plate at density of 1×10^5 . Twelve hours later, new culture medium was added to replace the previous one, then the compounds were added to the wells to achieve final concentrations. Upon completion of the incubation for 48 h, MTT dye solution (20 μL , 5 mg/mL) was added to each well. After 4 h incubation, all the solution inside each well was sucked out carefully and then added DMSO (150 μL) to solubilize the MTT formazan. The OD of each well was measured on a microplate spectrophotometer at a wavelength of 492 nm. The dose causing 50% inhibition of cell growth (IC_{50}) was determined from the curve of inhibiting percentage versus dose.

4.5. Cell apoptosis assay

The cervical carcinoma cells (Hela) in exponential phase were digested with trypsin, then seeded into a 12-well plate at density of 3×10^5 , and grown in an atmosphere of 5% CO_2 at 37 °C. Twelve hours later, new culture medium was added to replace the previous one, and then the compounds were added to the wells at the concentrations of 2, 100 and 200 μM , respectively. After 48 h of culture, cells were collected (including cells in culture medium and cells attached to the bottom of the bottle wall), then centrifuged and washed twice with PBS. Cells were re-suspended in 300 μL of binding buffer, and added 5 μL of FITC and 10 μL of PI to cells, and vortexed for a while. The cell suspension was incubated in the dark at 5–15 min at room temperature and then detected by flow

Table 3
Crystal data and structure refinement for compounds **1**, **3** and **5**.

Crystal data	1	3	5
Formula	C ₁₄ H ₂₀ ClNO ₂ Ru	C ₁₅ H ₂₁ ClNO ₂ Ru	C ₁₉ H ₂₂ ClNO ₂ Ru
M(g mol ⁻¹)	370.83	383.85	432.90
Crystal system	Monoclinic	Monoclinic	Monoclinic
Space group	P2(1)/n	P2(1)/n	P2(1)/c
a (Å)	8.5551(7)	9.4075(10)	12.9955(11)
b (Å)	12.5497(10)	13.0758(14)	7.4206(7)
c (Å)	14.6059(11)	13.5095(14)	19.7038(17)
α (deg)	90	90	90
β (deg)	101.0520(10)	97.910(2)	105.1830(10)
γ (deg)	90	90	90
Volume (Å ³)	1539.1(2)	1646.0(3)	1833.8(3)
Z	4	4	4
Density (Mg/m ³)	1.600	1.549	1.568
F000	752	780	880
Crystal size(mm ³)	0.20 × 0.10 × 0.10	0.20 × 0.20 × 0.10	0.20 × 0.10 × 0.10
Index ranges	-12 ≤ h ≤ 11 -18 ≤ k ≤ 18 -21 ≤ l ≤ 21	-13 ≤ h ≤ 13 -18 ≤ k ≤ 14 -19 ≤ l ≤ 19	-18 ≤ h ≤ 18 -10 ≤ k ≤ 10 -26 ≤ l ≤ 28
θ range(deg)	2.16 to 31.50	2.18 to 30.50	1.62 to 31.00
Completeness	98.0%	99.9%	99.4%
N (R _{int})	5029(0.0983)	5014(0.0903)	5815(0.1035)
Reflections collected	16854	17252	19347
Absorption coefficient(mm ⁻¹)	1.189	1.115	1.011
Max. and min	0.8903 and 0.7969	0.8967 and 0.8078	0.9057 and 0.8234
GOF on F ²	0.982	1.026	1.089
R ₁ , wR ₂ [I > 2σ(I)]	R ₁ = 0.0339 wR ₂ = 0.0669	R ₁ = 0.0455 wR ₂ = 0.1119	R ₁ = 0.0339 wR ₂ = 0.0823
R indices (all data)	R ₁ = 0.0475 wR ₂ = 0.0736	R ₁ = 0.0626 wR ₂ = 0.1211	R ₁ = 0.0424 wR ₂ = 0.0937

cytometry (Beckman coulter flow cytometry).

4.6. Cell cycle analysis

The cervical carcinoma cells (Hela) were digested in exponential phase with trypsin, then seeded into a 6-well plate at density of 3×10^6 , and grown in an atmosphere of 5% CO₂ at 37 °C. Twelve hours later, new culture medium was added to replace the previous one and then the compounds were added to the wells at the concentration of 100 μM. After 48 h of culture, the culture medium was discarded, and cells were collected by centrifugation. The cells was washed twice with PBS, and centrifuged. The PBS was discarded, and 300 μL of DNA staining solution and 10 μL of permeabilization solution were added it, then the cell suspension was vortexed and incubated for 30 min at 37 °C, then detected by flow cytometry.

4.7. Scratch wound healing assay

A vertical line with a marker pen was first drawn on the back of a 24-well plate for retained. Human hepatocellular carcinoma cells (HepG2) in exponential phase were digested with trypsin, then seeded into a 24-well plate (5×10^4 cells/well), and grown in 5% CO₂ at 37 °C for 12 h. Cells mono-layers were wounded with a sterile 100-μL pipette tip and washed with growth medium to remove detached cells from the plates and immediately photographed under a microscope. Cells were exposed to compounds-containing medium (not containing fetal bovine serum) at a concentration of 100 μM and incubated at 37 °C, saturated humidity, 5% CO₂ incubator, respectively, and the cells were photographed in 6 h and 24 h using an Olympus BX41 microscope (Tokyo, Japan) and a digital camera.

4.8. Transwell migration assay

Human hepatocellular carcinoma cells (HepG2) in exponential

phase were digested with trypsin and the medium was discarded by centrifugation, then washed 1–2 times with PBS and re-suspended with serum-free medium. Adjusting the cell density was adjusted into 8×10^4 /mL. Cell suspension with compounds (200 μL, not containing fetal bovine serum) at a concentration of 150 μM was added to transwell chamber (Costar USA). The medium containing 10% fetal bovine serum (500 μL) was added in 24-well plate, then incubated at 37 °C, saturated humidity and 5% CO₂ for 24 h. Cells were fixed 15 min with 4% paraformaldehyde, then wiped with a cotton swab on matrigel and transwell chamber. Then the cells in 24-well plate were stained with 0.3% crystal violet 10 min, then washed with saline after dyeing and photographed under a microscope.

4.9. Western blot analysis

HepG2 cells were harvested and lysed with RIPA lysis buffer by incubation on ice for 10 min. After centrifugation at 8000 rpm for 5 min, supernatants were collected and concentrations of proteins were measured using BCA reagent (purchased from Bio-Rad laboratories, USA). The protein samples were denatured by boiling at 95 °C for 5 min and loaded onto SDS-PAGE gel for electrophoresis. The proteins were transferred onto PVDF membranes and the membranes then incubated in the blocking solution (5% non-fat dried milk) at room temperature for 0.5 h and were then incubated with primary antibodies at 4 °C overnight. The membranes were subsequently incubated with secondary antibodies for 1 h. Protein expression was normalized against tubulin expression. Blotting images were acquired with the Odyssey infrared imaging system (Li-COR Biosciences, USA) and analyzed by the software provided by the manufacturer. Primary antibodies anti-Bcl-2 E-cadherin (proteintech, USA) anti-Bcl-2 Vimentin (proteintech, USA), anti-Cyclin-D1 (CST, USA) and anti-Cyclin-E1 antibody (Boster, Wuhan, China) were all used at a concentration of 1: 1000.

Supplementary materials

CCDC–1480620 (1), 1480631 (3), and 1480632 (5) contain the supplementary crystallographic data for this paper. These data can be obtained free of charge from the Cambridge Crystallographic Data Centre via www.ccdc.cam.ac.uk/data_request/cif.

Acknowledgments

This work has been supported by the National Natural Science Foundation of China (No: 81102311), the Natural Science Foundation of Hubei Province of China (No: 2016CFB433) and the Fundamental Research Funds for the Central Universities of China (No. 2015TS131).

References

- [1] B. Rosenberg, L. Van Camp, T. Krigas, *Nature* 205 (1965) 698–699.
- [2] E. Wong, C.M. Giandomenico, *Chem. Rev.* 99 (1999) 2451–2466.
- [3] M.J. Clarke, F. Zhu, D.R. Frasca, *Chem. Rev.* 99 (1999) 2511–2534.
- [4] S.J. Tan, Y.K. Yan, P.P.F. Lee, K.H. Lim, *Future Med. Chem.* 2 (2010) 1591–1608.
- [5] D. Chen, V. Milacic, M. Frezza, Q.P. Dou, *Curr. Pharm. Des.* 15 (2009) 777–791.
- [6] G. Sava, A. Bergamo, P.J. Dyson, *Dalton Trans.* 40 (2011) 9069–9075.
- [7] B.S. Murray, M.V. Babak, C.G. Hartinger, P.J. Dyson, *Coord. Chem. Rev.* 306 (2016) 86–114.
- [8] Z. Adhireksan, G.E. Davey, P. Campomanes, M. Groessler, C.M. Clavel, U. Rothlisberger, P.J. Dyson, H. Yu, P. Droge, A.A. Nazarov, C.H.F. Yeo, W.H. Ang, C.A. Davey, *Nat. Commun.* 5 (2014) 3462.
- [9] C.G. Hartinger, N. Metzler-Nolte, P.J. Dyson, *Organometallics* 31 (2012) 5677–5685.
- [10] B. Wu, M.S. Ong, M. Groessler, Z. Adhireksan, C.G. Hartinger, P.J. Dyson, C.A. Davey, *Chem. Eur. J.* 17 (2011) 3562–3566.
- [11] P. Nowak-Sliwinska, J.R. van Beijnum, A. Casini, A.A. Nazarov, G. Wagnieres, H. van den Bergh, P.J. Dyson, A.W. Griffioen, *J. Med. Chem.* 54 (2011) 3895–3902.
- [12] M.J. Chow, C. Licon, D.Y.Q. Wong, G. Pastorin, C. Gaiddon, W.H. Ang, *J. Med. Chem.* 57 (2014) 6043–6059.
- [13] A. Grozav, O. Balacescu, L. Balacescu, T. Cheminel, I. Berindan-Neagoe, B. Therrien, *J. Med. Chem.* 58 (2015) 8475–8490.
- [14] (a) G. Sava, S. Zorzat, C. Turrin, F. Vita, M. Soranzo, G. Zabucchi, M. Cocchiello, A. Bergamo, S. DiGiovine, G. Pezzoni, L. Sartor, S. Garbisa, *Clin. Cancer Res.* 9 (2003) 1898–1905; (b) J.M. Rademaker-Lakhai, D. van den Bongard, D. Pluim, J.H. Beijnen, J.H.M. Schellens, *Clin. Cancer Res.* 10 (2004) 3717–3727.
- [15] C.G. Hartinger, M.A. Jakupec, S. Zorbas-Seifried, M. Groessler, A. Egger, W. Berger, H. Zorbas, P.J. Dyson, B.K. Keppler, *Chem. Biodivers.* 5 (2008) 2140–2155.
- [16] P.S. Kuhn, V. Pichler, A. Roller, M. Hejl, M.A. Jakupec, W. Kandioller, B.K. Keppler, *Dalton Trans.* 44 (2015) 659–668.
- [17] W.H. Ang, P.J. Dyson, *Eur. J. Inorg. Chem.* (2006) 4003–4018.
- [18] A.F.A. Peacock, P.J. Sadler, *Chem. Asian J.* 3 (2008) 1890–1899.
- [19] (a) B.S. Murray, M.V. Babak, C.G. Hartinger, P.J. Dyson, *Coord. Chem. Rev.* 306 (2016) 86–114; (b) B. Wu, M.S. Ong, M. Groessler, Z. Adhireksan, C.G. Hartinger, P.J. Dyson, C.A. Davey, *Chem. Eur. J.* 17 (2011) 3562–3566; (c) A. Bergamo, C. Gaiddon, J.H.M. Schellens, J.H. Beijnen, G. Sava, *J. Inorg. Biochem.* 106 (2012) 90–99.
- [20] X. Shang, T.F.S. Silva, L.M.D.R.S. Martins, Q. Li, M.F.C.G. da Silva, M.L. Kuznetsov, A.J.L. Pombeiro, *J. Organomet. Chem.* 730 (2013) 137–143.
- [21] K.J. Gotink, H.M.W. Verheul, *Angiogenesis* 13 (2010) 1–14.
- [22] O. Schmalhofer, S. Brabletz, T. Brabletz, *Cancer Metastasis Rev.* 28 (2009) 151–166.
- [23] N. Bandyopadhyay, M. Zhu, L. Lu, D. Mitra, M. Das, P. Das, A. Samanta, J.P. Naskar, *Eur. J. Med. Chem.* 89 (2015) 59–66.
- [24] J. Custot, J.L. Boucher, S. Vadon, C. Guedes, S. Dijols, M. Delaforge, D. Mansuy, *J. Biol. Inorg. Chem.* 1 (1996) 73–82.
- [25] N. Chitrapriya, V. Mahalingam, M. Zeller, H. Lee, K. Natarajan, *J. Mol. Struct.* 984 (2010) 30–38.
- [26] Y. Benabdelouahab, L. Muñoz-Moreno, M. Frik, I. de la Cueva-Aliques, M.A.E. Amrani, M. Contel, A.M. Bajo, T. Cuenca, E. Royo, *Eur. J. Inorg. Chem.* (2015) 2295–2307.
- [27] N. Chitrapriya, V. Mahalingam, L.C. Channels, M. Zeller, F.R. Fronczek, K. Natarajan, *Inorg. Chim. Acta* 361 (2008) 2841–2850.
- [28] R. Pettinari, F. Marchetti, C. Pettinari, A. Petrini, R. Scopelliti, C.M. Clavel, P.J. Dyson, *Inorg. Chem.* 53 (2014) 13105–13111.
- [29] M. Watanabe, Y. Kashiwame, S. Kuwata, T. Ikariya, *Chem. Lett.* 39 (2010) 758–759.
- [30] A.K. Barui, V. Veeriah, S. Mukherjee, J. Manna, A.K. Patel, S. Patra, K. Pal, S. Murali, R.K. Rana, S. Chatterjee, C.R. Patra, *Nanoscale* 4 (2012) 7861–7869.
- [31] Z.M. Wang, L.N. Ji, *Prog. Chem.* 14 (2002) 296–304.
- [32] C.M. Franz, G.E. Jones, A.J. Ridley, *Dev. Cell* 2 (2002) 153–158.
- [33] P. Friedl, K. Wolf, *Nat. Rev. Cancer* 3 (2003) 362–374.
- [34] J.Y. Chen, Y.A. Tang, S.M. Huang, H.F. Juan, L.W. Wu, Y.C. Sun, S.C. Wang, K.W. Wu, G. Balraj, T.T. Chang, W.S. Li, H.C. Cheng, Y.C. Wang, *Cancer Res.* 71 (2011) 473–483.
- [35] A. Albin, *Pathol. Oncol. Res.* 4 (1998) 230–241.
- [36] S. Zorzat, A. Bergamo, M. Cocchiello, A. Sorc, B. Gava, E. Alessio, E. Iengo, G. Sava, *J. Pharmacol. Exp. Ther.* 295 (2000) 927–933.
- [37] A. Satelli, S. Li, *Cell. Mol. Life Sci.* 68 (2011) 3033–3046.
- [38] J.P. Thiery, H. Acloque, R.Y.J. Huang, M.A. Nieto, *Cell* 139 (2009) 871–890.
- [39] M.A. Bennett, A.K. Smith, *Dalton Trans.* (1974) 233–241.
- [40] L.K. Johnson, Iron or cobalt complex catalyst for polymerization of ethylene, *PCT Int. Appl.* (2000), 2000066638.
- [41] A.M. Radwan, E.E. Eslam, R. Kassab, M.H. Elnagdi, *J. Chem. Soc. Pak.* 18 (1996) 166–169.
- [42] G.M. Sheldrick, SHELXTL-97, Program for X-ray Crystal Structure Solution and Refinement, Göttingen University, Germany, 1997.
- [43] C.M. Schempp, V. Kirkin, B. Simon-Haarhaus, A. Kersten, J. Kiss, C.C. Termeer, B. Gilb, T. Kaufmann, C. Borner, J.P. Sleeman, J.C. Simon, *Oncogene* 21 (2002) 1242–1250.